NANO LETTERS

Letter

pubs.acs.org/NanoLett

Strain-Induced Band Gap Engineering in Selectively Grown GaN–(Al,Ga)N Core–Shell Nanowire Heterostructures

Martin Hetzl,*[,†] Max Kraut,[†] Julia Winnerl,[†] Luca Francaviglia,[‡] Markus Döblinger,[§] Sonja Matich,[†] Anna Fontcuberta i Morral,[‡] and Martin Stutzmann*[,†]

[†]Walter Schottky Institut and Physics Department, Technische Universität München, 85748 Garching, Germany

[‡]Laboratoire des Matériaux Semiconducteurs, École Polytechnique Fédérale de Lausanne, 1015 Lausanne, Switzerland

[§]Department of Chemistry, Ludwig-Maximilians-Universität München, 81377 Munich, Germany

Supporting Information

ABSTRACT: We demonstrate the selective area growth of GaN–(Al,Ga)N core–shell nanowire heterostructures directly on Si(111). Photoluminescence spectroscopy on as-grown nanowires reveals a strong blueshift of the GaN band gap from 3.40 to 3.64 eV at room temperature. Raman measurements relate this shift to compressive strain within the GaN core. On the nanoscale, cathodoluminescence spectroscopy and scanning transmission electron microscopy prove the homogeneity of strain-related luminescence along the nanowire axis and the absence of significant fluctuations within the shell, respectively. A comparison of the experimental findings with numerical simulations indicates the absence of a significant defect-related strain relaxation for all investigated structures, with a maximum compressive strain of −3.4% for a shell thickness of 50 nm. The accurate control of the nanowire dimensions, namely, core diameter, shell thickness, and nanowire period, via selective area growth allows a specific manipulation of the resulting strain within individual nanowires on the same sample. This, in turn, enables a spatially resolved adjustment of the GaN band gap with an energy range of 240 meV in a one-step growth process.

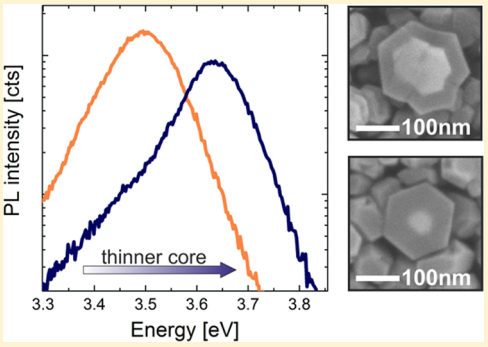

KEYWORDS: *Nanowires, core–shell, heteroepitaxy, selective area growth, strain, photoluminescence, Raman scattering, cathodoluminescence, band gap engineering*

Over the past decade, group III-nitride nanowires (NWs) have gained much interest. Thanks to their high crystal quality and the possibility to grow on various substrates,[1−4] NWs are a promising alternative to thin films for optoelectronic devices such as LEDs or laser diodes.[5,6] However, the radiative recombination efficiency drops compared to thin films.[7] This has been assigned to nonradiative recombination paths at surface states, which appear to be a significant factor for NWs due to their high surface-to-volume ratio. In addition, these surface states are responsible for a diameter-dependent depletion of charge carriers within the NW due to Fermi level pinning, which reduces the performance of electrically driven NW-based devices.[8−10] A possible way to overcome this problem is to passivate the surface by a several nanometers of thin shell consisting of (Al,Ga)N.[11] Moreover, GaN/(Al,Ga)N core–shell NWs can be beneficial compared to axial heterostructures in the context of nonpolar quantum wells since they exclude the presence of an internal electric field.[12] In the present work, we concentrate on the lattice mismatch between the GaN NW core and the (Al,Ga)N shell, which induces strain in particular along the NW axis and thereby affects the electronic band structure. Rigutti et al. have shown a strain-induced blueshift of the band gap emission of ∼60 meV for self-assembled GaN–AlN core–shell NWs.[13] However, due to the statistical nature of the self-assembled growth process, namely, fluctuating nucleation densities and strong variations in the core diameter, their studies were limited to a variation of the shell thickness by only 5 nm. For thicker shells, Hestroffer et al. have shown that inhomogeneous nucleation due to shadowing of neighboring NWs induces defects and strain gradients.[12] This can be avoided by selective area epitaxy, providing an accurate control of both NW diameter and density.

In this letter, we present a highly controllable way of strain-induced band gap engineering of GaN NWs via heteroepitaxial selective area growth (SAG) of GaN–(Al,Ga)N core–shell NW heterostructures on Si(111), which allows the tuning of the GaN band gap from 3.40 up to 3.64 eV at room temperature and the option of a spatial variation of the band gap within this spectral region in a one-step growth process. A systematic study of the SAG core–shell growth is presented where we address in detail the variation of the core diameter, the influence of the shell thickness, the period of the NW arrays, and the alloy composition of the shell. Moreover, the

Received: August 10, 2016
Revised: October 19, 2016
Published: October 21, 2016

DOI: 10.1021/acs.nanolett.6b03354
Nano Lett. 2016, 16, 7098−7106

experimental findings are compared to 2D numerical simulations of the appearing strain and the resulting modifications of the electronic band structure.

Selective Nanowire Growth. The samples investigated in this work are grown by plasma-assisted molecular beam epitaxy (MBE) directly on n-Si(111) substrates in a SAG process with the help of a structured titanium nitride mask. This allows an accurate control of both, NW diameter and period. In particular, 10 nm of Ti has been thermally evaporated on the Si substrate and subsequently covered by a positive e-beam resist. Then, hexagonal arrays of holes of different diameter and period have been implemented into the resist by e-beam lithography and transferred into the Ti film by wet chemical etching to reveal the bare Si substrate. A detailed description of the substrate preparation can be found elsewhere.[14,15] Prior to growth, the sample surface has been exposed to a N plasma within the MBE chamber at a substrate temperature T_{sub} = 400 °C to convert the Ti mask into thermally more stable TiN.[16] The GaN core growth takes place under highly N-rich growth conditions at T_{sub} = 850 °C, which is located about 40 K below the optimum substrate temperature for self-assembled GaN NWs.[14] Note that these values refer to thermal couple measurements of the heater. After 90 min of growth a NW length of ∼600 nm has been reached. The subsequent shell growth has been realized at a slightly decreased T_{sub} = 830 °C to achieve lateral NW growth. The Al and Ga flux have been readjusted to obtain a distinct alloy composition, whereas the effective III/V-flux ratio has been kept constant for both core and shell growth. The growth parameters for the desired alloy compositions have been obtained from (Al,Ga)N reference layers on GaN template, grown under equivalent effective T_{sub} and III/V-flux ratio. The alloy composition in these reference layers has been measured by high-resolution X-ray diffraction. A consistent study of the alloy-dependent (Al,Ga)N defect luminescence of the core−shell NWs can be found in the Supporting Information. Note that no intermediate buffer layer between the mask and the Si substrate has been used for the SAG of GaN NWs to prevent unintended buffer layer luminescence during optical characterization.

In Figure 1, scanning electron microscopy (SEM) images of different NW arrays are shown in 45° tilted view. As a reference sample for the core, pure GaN NWs with a period of 500 nm and a diameter of 60 nm are displayed in Figure 1a. The as-grown NWs are characterized by a uniform shape and the absence of parasitic growth on the mask surface. Obviously, some NWs show a slight tilting with respect to the substrate normal, which has already been observed in previous work for heteroepitaxial SAG and also for self-assembled growth on Si(111). This has been assigned to an intermediate Si_xN_y layer of several nanometers between the Si substrate and the GaN NWs leading to an imperfect epitaxial relationship between both crystals.[14,17] The mask has been fabricated with different array configurations. In particular, GaN cores have been simultaneously grown on each sample with array sizes of 100 × 100 μm^2 and a spacing of 200 μm, with NW diameters ranging from 40 to 170 nm and periods from 300 to 2000 nm. In this way, a maximum amount of information and comparability can be obtained for a small number of growth cycles. In Figure 1b,c, equivalent arrays as in Figure 1a but with additional nominal shell thicknesses of 20 and 65 nm are shown, respectively. Note that the nominal shell thickness values have been obtained from top-view SEM images on these particular arrays by subtracting the core diameter of the GaN

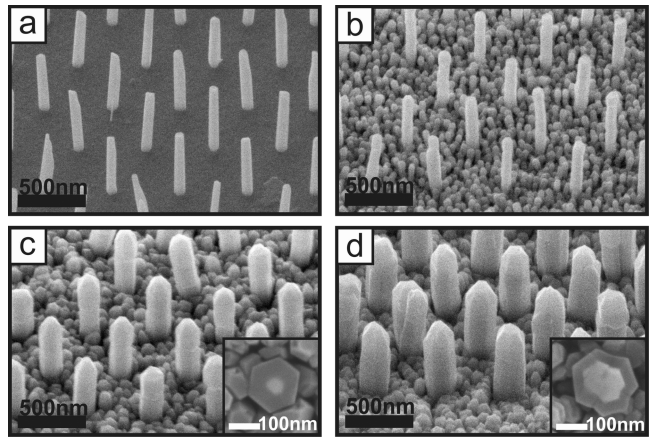

Figure 1. Tilted view SEM images (45°) of (a) pure SAG GaN NWs on Si(111) (sample A), (b,c) GaN−(Al,Ga)N core−shell NWs with different shell thickness (samples C and D), and (d) a thicker core with similar shell as in (c) (sample D). An overview of the mentioned samples can be found in Table 1. The insets in (c) and (d) refer to top view SEM images of remaining core−shell pillars after the NW releasing step.

reference sample (Figure 1a). On both samples, parasitic growth can be observed on the mask, which is a result of the decreased T_{sub} and the higher sticking coefficient of Al atoms during shell growth.[18] Since the parasitic nucleation consists solely of shell material, no considerable contribution to the following analysis of the core−shell NWs is expected (Supporting Information). Concerning the actual shell nucleation at the GaN NWs, a closed overgrowth can be estimated already for the 20 nm shell sample. At the NW top facets pronounced caps are visible, which seem to have a larger diameter as the underlying structure (Figure 1b). Thus, the given nominal shell thickness tends to overestimate the real value. In the case of the thicker shell (Figure 1c), a homogeneous and smooth nucleation along the NW sidewalls can be observed, which is an important requirement to guarantee representative optical measurements over a large scale. For comparison, an array from the same sample as in Figure 1c, but with larger core diameter of ∼120 nm is shown in Figure 1d. Here, multiple nucleation of the core within the TiN mask holes can take place, where the separated crystallites merge together during growth. Despite this inhomogeneity for larger core diameters, a closed and homogeneous nucleation of the shell is still occurring. An overview of all samples fabricated for this study is listed in Table 1 including sample number, nominal shell thickness, and intentional Al content of the shell.

Table 1. List of Investigated NW Samples on Si(111)[a]

sample	shell thickness [nm]	Al content [%]
A	0	0
B	6	95
C	20	95
D	65	95
E	65	100
F	65	80

[a]Each sample contains a set of array dimensions, i.e., periods and diameters. The shell thicknesses refer to nominal values measured by top-view SEM images. The Al content has been determined from reference layers.

DOI: 10.1021/acs.nanolett.6b03354
Nano Lett. 2016, 16, 7098−7106

Experimental Techniques. Optical measurements have been performed by means of room temperature μ-photoluminescence spectroscopy (PL). A frequency quadrupled Nd:YAG laser resulting in a wavelength of 266 nm in continuous wave operation has been used to radiatively excite the GaN core above the band gap. To distinguish between different types of arrays and to measure a large enough ensemble of NWs for statistics the laser beam has been focused to a spot size of several micrometers directly on as-grown NWs, i.e., the incident beam is parallel to the NW axis. Due to a thick defective cap of (Al,Ga)N at the top facet (not further discussed in this letter) and the decreased incoupling efficiency for this sample geometry, an excitation intensity of 30 kW/cm^2 has been chosen for all measurements to obtain enough signal from the core. Note that no significant temperature-induced redshift has been observed for this excitation power. The emitted light from the NWs has been collected in a DILOR double spectrometer with a focal length of 80 cm and a spectral resolution of 0.05 nm and was detected by a Peltier-cooled photomultiplier tube.

μ-Raman measurements have been performed at room temperature with a 532 nm excitation wavelength and a spot size of ~1 μm on as-grown NWs under backscattering geometry. The scattered light has been captured by a triple DILOR spectrometer with 1200 l/mm gratings and was detected by a LN2-cooled CCD camera with a resolution of 0.5 cm^{-1}.

Cathodoluminescence spectroscopy (CL) has been realized with an Attolight SEM-CL microscope, operated at room temperature under UHV conditions. An acceleration voltage of 7 kV results in a large interaction volume with a penetration depth of ~200 nm. Following Monte Carlo simulations with the free software CASINO, it can be assumed that 50% of the CL signal is emitted from an area of 10 nm around the incident electron beam, which provides a good spatial contrast on the nanoscale (Supporting Information). The emitted light from the NWs has been captured by a dispersive spectrometer with a focal length of 32 cm and a grating of 150 l/mm and detected by a Peltier-cooled CCD camera, resulting in a spectral resolution of 1.6 nm. To measure CL along the NW growth axis, the NWs have been released from their nucleation sites by means of an atomic force microscope (AFM) in contact mode. In contrast to conventional releasing techniques, this method has the advantage that scratched off NWs remain near their original location, which is especially important for assignment to a specific array type. Due to parasitic growth on the mask, the cleave edge typically appears about 100−200 nm above the NW onset, which leaves behind a characteristic pillar where both core and shell can be distinguished by SEM (Figure 1c,d insets).

Scanning transmission electron microscopy (STEM) has been performed with a FEI-TITAN microscope at an acceleration voltage of 300 kV. To guarantee electron transparency the investigated core−shell NWs have been thinned from both sides by a Zeiss NVISION40 focused ion beam (FIB) system.

Results and Discussion. In Figure 2, room temperature PL spectra of the near-band-edge emission of GaN are plotted for different core diameters (sample D, Table 1) for a fixed NW period of 500 nm and an intentional shell thickness of 65 nm. A PL spectrum of pure GaN NWs is included for comparison (sample A, Table 1). In this temperature regime, the main contribution to this peak is recombination of free excitons.[19]

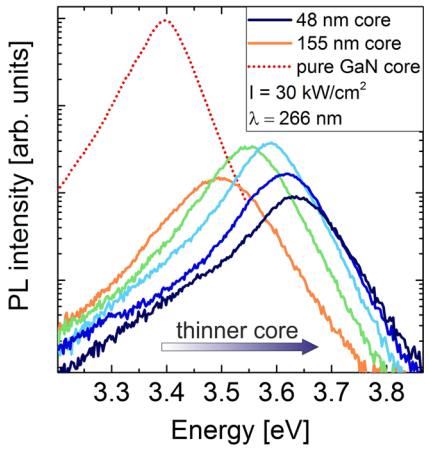

Figure 2. Room temperature PL spectra of GaN−(Al,Ga)N core−shell NWs with varying core diameter: 48, 60, 78, 120, and 155 nm. The corresponding NW arrays are grown with a 65 nm $Al_{95}Ga_5N$ shell (sample D, Table 1). A PL spectrum of pure GaN NWs (60 nm diameter) is included for comparison (sample A, Table 1).

This is also taken into consideration for the numerical simulations section further below. The absolute PL signal of the core−shell structures decreases with respect to the GaN NWs by about two orders of magnitude. A possible reason could be the observed nucleation of a ~250 nm thick defective (Al,Ga)N cap on the NW top facet during shell growth, which effectively attenuates the incident laser beam. A brief overview of the occurring defect luminescence within the (Al,Ga)N is shown in the Supporting Information. However, the investigation of defects within the shell and its role for the overall PL spectrum will be addressed in a different publication. For increasing core diameter the peak intensity increases at first by a factor of four, reaches a maximum for diameters of the order of 100 nm, and decreases again for even higher ones. The initial increase can be easily understood by a higher core volume being excited. The intensity drop for largest diameters could be a geometrical effect: Since the free space in between the separate core−shell NWs becomes smaller, the contribution of absorbed light injected over the sidewalls becomes less pronounced. A more prominent feature of the measured spectra is the observed strong energy shift of the peak maxima for different core diameters. In particular, the thinnest core shows a maximum blueshift of ~240 meV with respect to the GaN reference value of 3.393 eV, whereas a blueshift of ~100 meV has been observed for a 155 nm core diameter. The respective core−shell peaks show similar full width at half-maxima (FWHMs) of around 100 meV. Compared to a FWHM of 80 meV of pure GaN this indicates a high uniformity of radiative emission of the grown core−shell structures. Worth mentioning is a characteristic shoulder on the low energy tail particularly for smaller core diameters. This could be explained by a small fraction (~1%) of unstrained regions in the NW ensemble investigated. A second possible explanation is a defect-related luminescence in the (Al,Ga)N shell observed in CL. However, this emission is almost two orders of magnitude weaker compared to the main peak.

For a quantitative investigation of the observed blueshift, NWs of varying shell thickness but equivalent alloy concentrations and NW period have been measured (samples B, C, and D, Table 1). The energetic positions of the peak maxima of the respective PL emissions obtained by a Gaussian

DOI: 10.1021/acs.nanolett.6b03354
Nano Lett. 2016, 16, 7098−7106

fit are illustrated in Figure 3a as a function of the core diameter. For all samples an almost linear decrease of the PL energy with

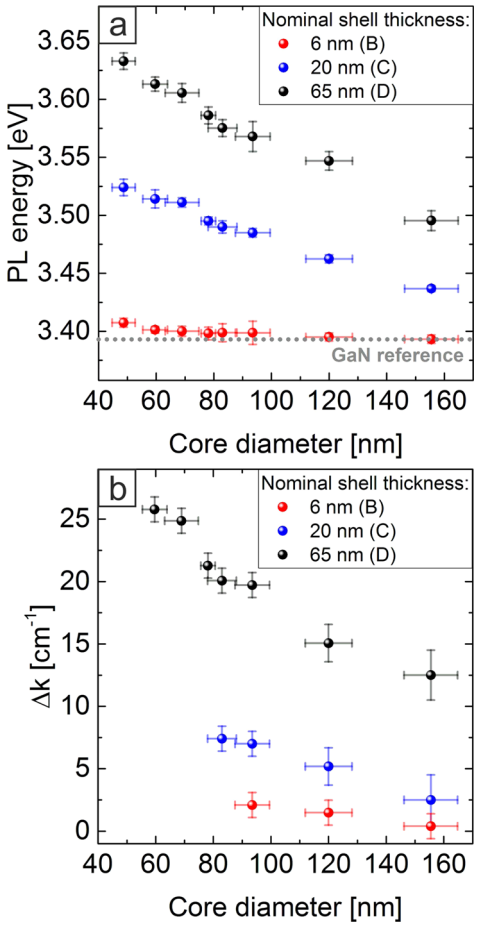

Figure 3. (a) Room temperature PL peak energies and (b) wavenumber shift Δk of the E_2^{high} Raman mode of GaN as a function of core diameter for different nominal shell thicknesses. The respective sample specifications are listed in Table 1.

increasing diameter can be observed, whereas the corresponding slope and absolute energy variation increase for higher shell thicknesses. In particular, the energetic difference between the smallest and largest diameter amounts to 90 and 140 meV for the medium and thick shell, respectively, whereas for the very thin shell the shift is less uniform and pronounced (ΔE = 15 meV). According to the literature, this shift results from lattice mismatch-induced strain between the GaN core and (Al,Ga)N shell.[13] To prove this assumption μ-Raman measurements have been performed on the same samples at room temperature. In particular, the E_2^{high} mode of GaN is known to be sensitive to strain within the crystal lattice.[20] Thus, the energetic shift of the E_2^{high} mode, i.e., $\Delta k = k(E_2^{high,ex}) - k(E_2^{high,0})$, of the respective core–shell NW arrays is plotted in Figure 3b as a function of the core diameter. As a reference for unstrained GaN a value of $k(E_2^{high,0})$ = 572.5 cm^{-1} has been obtained from sample A (Table 1). As a result, the energy shifts Δk show qualitatively a similar behavior as the PL peak energies (Figure 3a) with a maximum shift for the thickest shell (65 nm) and a 60 nm core of Δk = 26 cm^{-1}. For thinner shells also the overall Raman shift decreases but remains linear with respect to the core diameter. These findings are in contrast to observations of Hestroffer et al., who have investigated self-assembled GaN–AlN core–shell NWs by Raman spectroscopy. Due to the lack of nucleation control a saturation of the E_2^{high} mode for shell thicknesses larger than 3 nm has been reported, whereas in the present case no such saturation could be observed. Note that the thinnest core diameters (48 nm) cannot be measured due to an insufficient incoupling of the Raman laser. In the literature, a blueshifted E_2^{high} mode corresponds to compressive strain along the GaN core induced by different lattice parameters of GaN (5.185 Å) and AlN (4.982 Å) in *c*-direction.[12,21] Since both Raman and PL measurements coincide qualitatively with each other it can be concluded that compressive strain is also the main reason for the change in the measured band gap emission (Figure 3a).

Up to now, the focus has been on the dimensions of the core–shell structure, i.e., the variation of core diameter and shell thickness. In the following the influence of the NW period as well as the alloy composition of the shell will be discussed in terms of morphology and optical characteristics. To assess the influence of the NW period on the PL emission, 500 nm arrays are compared to arrays with a period of 300 nm grown on the same sample. In Figure 4a the corresponding PL peak energies

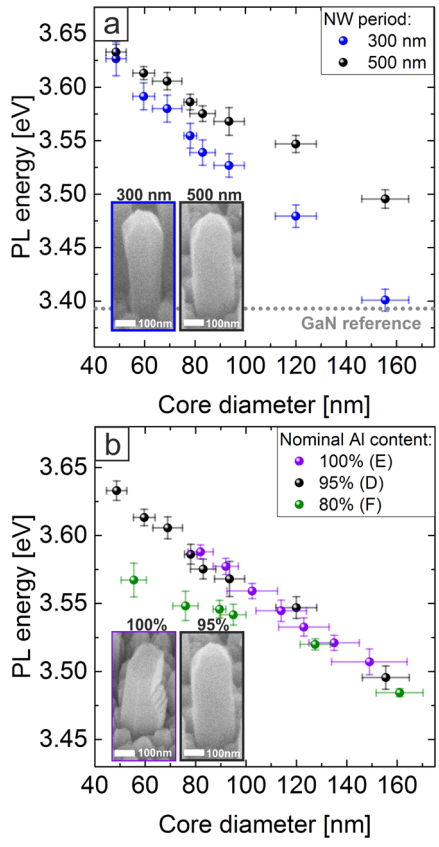

Figure 4. PL peak energies as a function of core diameter for (a) different NW period with an Al content of 95% and (b) different nominal alloy compositions of the shell for a fixed NW period of 500 nm. The respective sample specifications are listed in Table 1.

are illustrated as a function of the core diameter in the case of a thick shell (sample D, Table 1). For small core diameters the energy shift with respect to the pure GaN reference is the same within experimental accuracy. However, for increasing core diameters the peak energies of 300 and 500 nm periods diverge: The shift for the array with 300 nm period is consistently smaller and approaches the pure GaN band gap for the largest

DOI: 10.1021/acs.nanolett.6b03354
Nano Lett. 2016, 16, 7098–7106

core. In the insets of Figure 4a, exemplary core−shell NWs related to the different periods are shown. While the 500 nm case has already been discussed before, a clear cone shape can be identified for the 300 nm period, with a tapering toward the bottom. The origin of this difference can be found in the particular growth mechanism of SAG. During MBE growth of the core, impinging Ga atoms are able to diffuse on the substrate as well as on the NW sidewalls within a characteristic diffusion length before being either incorporated into the crystal or desorbed.[22] This results in the well-known NW shape. However, due to the decreased T_{sub} during shell growth and the higher sticking coefficient of Al, a strong decrease of the diffusion length can be expected.[1] This leads to an incorporation of group III atoms in the direct vicinity of their impact. As a consequence of the chamber geometry where the atomic beams arrive at an angle of ∼30° with respect to the substrate normal, shadowing effects of neighboring NWs occur, which is more pronounced in the lower part of the NWs. This leads to the observed cone shape of dense core−shell NW arrays. Since the occurring strain is influenced by the shell thickness (Figure 3a), the resulting band gap is expected to vary along the NW in this case, which leads to an effective decrease of the measured PL peak energy as well as broadened FWHMs of ∼130 meV (not shown).

For all previous samples, the alloy composition of the shell has been adjusted to 95% Al content. Naturally, different alloy compositions are expected to influence the strain within the core−shell system due to a change in the lattice mismatch at the interface. To elucidate this, different compositions of the shell of 80, 95, and 100% Al content have been investigated by PL (samples D, E, and F, Table 1) for a fixed NW period of 500 nm and a fixed shell thickness. The peak energies are plotted in Figure 4b as a function of the core diameter. Indeed, for a lower Al content of nominally 80% (sample F, Table 1) an overall decrease of the strain-induced blueshift occurs with respect to the 95% sample. In the case of a pure AlN shell (sample E, Table 1) the resulting PL peak energies cannot be distinguished from the 95% sample. However, a distinct change in the NW morphology has been observed in this case (Figure 4b, inset). In particular, the AlN shell is characterized by a strong inhomogeneous faceting on both the top and the sidewalls of the NW, probably induced by a defective overgrowth. Consequently, already small amounts of Ga seem to act as a surfactant for well-shaped GaN−(Al,Ga)N core−shell NW growth. Despite the inhomogeneous overgrowth the blue-shifted PL emission is following its expected trend. One possible explanation could be the appearance of two-dimensional defects mainly perpendicular to the growth axis, which would have no direct effect on the strain along the *c*-direction.

To clarify possible variations of the shell-induced strain inside a NW, investigations on the nanoscale are necessary. For that, CL measurements have been performed on a released core−shell NW with a core diameter of ∼48 nm from sample D (Table 1). In Figure 5a, a top view SEM image of the corresponding NW is displayed. The smaller structures beneath the NW are parasitic (Al,Ga)N nucleation sites on the mask due to the mentioned shell growth process. Note that the upper left end of the NW belongs to the top facet of the NW, identified by a characteristic tapering within the first 100 nm. For clarity the location and size of the core is indicated by dashed lines. In Figure 5b, the corresponding CL map of the near-band-edge emission of the core area is depicted in false colors. "Green" refers to the detected intensity at a photon

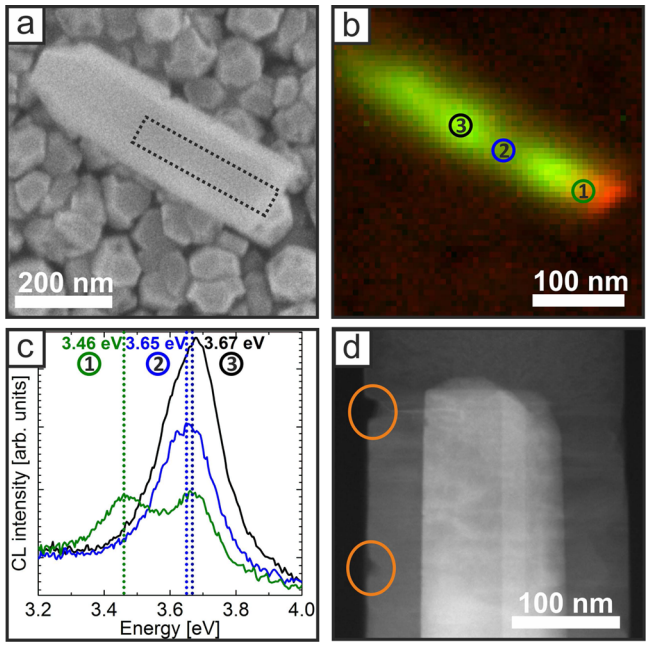

Figure 5. (a) SEM image of a released core−shell NW. The location of the core is marked with dashed lines. (b) Magnified CL map of the core in false colors. Green and red corresponds to the 3.67 and 3.46 eV emission, respectively. (c) CL intensity as a function of photon energy for three distinct locations in (b). (d) Cross-sectional HAADF STEM image of the upper core−shell area. The cracks along the shell surface are marked with orange circles.

energy of 3.67 eV, whereas "red" is attributed to 3.46 eV emission. Worth mentioning is a blueshift of 20−30 meV for the main CL emission peak with respect to PL measurements. This can be attributed to band filling effects within the GaN due to the strong electron excitation of ∼800 pA at 7 kV.[23] Perpendicular to the NW axis, i.e., along a cross-section through the heterostructure, the emission is characterized by a constant signal in both energy and intensity. A slight attenuation toward the core−shell interface can be assigned to an effective decrease of excited core volume due to the cylindrical geometry of the core. However, distinct deviations along the NW axis can be observed. For a quantitative analysis of these phenomena, the CL emissions of three distinct sites along the NW are plotted as a function of the photon energy in Figure 5c, where the corresponding locations are indicated by numbered circles in Figure 5b. The most prominent emission feature might be associated with the area near the bottom facet. Besides the 3.67 eV emission from the strained NW, another peak emerges at 3.46 eV. Thus, the color gradient in the CL map (Figure 5b, region 1) cannot be assigned to an energy shift but to a locally arising second emission at the bottom facet of the NW. A possible explanation is the specific structure of this core−shell NW: Due to the releasing of the NWs from their original substrates the GaN core is not encapsulated by any shell at the bottom facet. Thus, a local relaxation of the core occurs in this region, which is accompanied by a distinct redshift toward the unstrained GaN band gap. Since the NW is cut at a certain height of around 100−200 nm above its original bottom, a possible defect emission assigned to the nucleation stage can be excluded. In addition, this emission line has not been observed for as-grown NWs (not shown), which confirms the open cleavage facet to be responsible for this effect.

DOI: 10.1021/acs.nanolett.6b03354
Nano Lett. 2016, 16, 7098−7106

Another feature appears when going from the top facet of the NW toward the bottom. In particular, fluctuations associated with a decrease of the CL intensity by ~50% occur (regions 2 and 3). This effect is accompanied by a slight redshift of the main peak by about 20 meV. Note that all emission characteristics have been observed on numerous NWs investigated for this study. To clarify the origin of these fluctuations STEM measurements have been performed on a GaN−(Al,Ga)N core−shell NW equivalently grown as sample D (Table 1). In Figure 5d, a cross-sectional high-angle annular dark field (HAADF) STEM image of the upper core−shell region is displayed. A pronounced and sharp change of the contrast at the core−shell interface indicates an abrupt transition with no significant alloy gradients in this region. Thus, a variation of strain due to different alloying in the shell can be ruled out as an origin for the measured energy fluctuations in CL (Figures.5b,c). However, small cracks at the outer shell area with a depth of ~10 nm have been identified (marked with orange circles). One possible origin could be damaging of the core during thinning of the NW by FIB. However, the formation of cracks has also been reported for GaP-Si core−shell NWs, where thermal fluctuations accompanied by different thermal expansion coefficients have been proposed as a cause of the cracking.[24] As a consequence, these cracks effectively decrease the local shell thickness and thus can be responsible for an attenuation of strain in this area, leading to the observed energy fluctuations in CL. In this case, we would also expect an increase in luminescence intensity close to the cracks due to carrier capture in the resulting lower band gap region. This, however, is not observed. Our current explanation for this discrepancy is that the region around the cracks also contains electronic defects acting as nonradiative recombination centers. However, this point requires further investigation in the future. In addition, distinct lines within the shell perpendicular to the GaN sidewalls are visible in Figure 5d, which might be associated with defects or grain boundaries. However, since the predominant strain evolves from the lattice mismatch in *c*-direction these orthogonally oriented defects should have a minor influence on the resulting compression of the core. Note that the (Al,Ga)N shell shows a weak but constant defect emission along each NW, which underlines the high uniformity of the core−shell NW strain system. A corresponding CL spectrum of the shell as well as a high-resolution STEM study of the core−shell interface are shown in the Supporting Information.

As a result, the measurements on the nanoscale by CL spectroscopy confirm the findings obtained by PL and Raman. The observed fluctuations due to uncertainties of the shell surface are small compared to the overall strain-induced blueshifts, which allow a general theoretical consideration of the investigated GaN−(Al,Ga)N NW heterostructures.

Numerical Simulations. To compare our experimental findings with theoretical expectations, two-dimensional numerical band structure simulations of the GaN−(Al,Ga)N core−shell structures have been conducted. For this purpose, the nextnano[3] software package has been used to calculate the existing strain by a numerical strain solver minimizing the elastic energy in the system.[25] The resulting band structure is then calculated by solving the Poisson and drift-diffusion-current equation self-consistently in a Newton−Raphson algorithm. The simulation region is limited to the radial cross section of the core−shell NWs, whereas the length of the NWs has been assumed to be infinite. Since strain can be regarded as a purely classical influence on the band structure and the recombination efficiency is not in the focus of this work, quantum mechanical calculations have not been considered in the following. Deformation potentials and electronic band parameters have been adopted from the nextnano[3] database, which follows the publications of Vurgaftman and Ambacher et al. concerning nitrides.[21,26,27] Note that the band gap for the simulations has been adjusted to reproduce PL measurements of unstrained GaN to 3.393 eV at room temperature. To obtain a reasonable band bending at the heterointerfaces the n-type doping concentration for not intentionally doped (n.i.d.) GaN and (Al,Ga)N has been set to 1×10^{17}cm^{-3} mainly due to oxygen impurities.

In Figure 6a, the band structure across the center of the core of a coaxial GaN−$Al_{95}Ga_5N$ core−shell NW is plotted for a

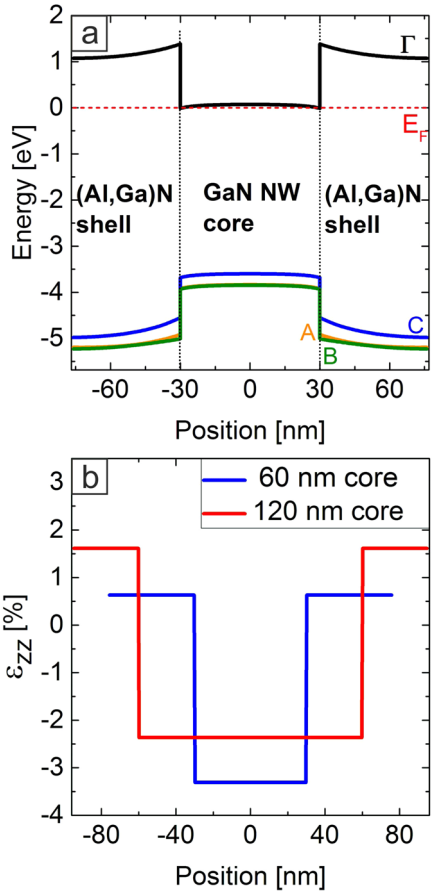

Figure 6. (a) Simulated band structure of a GaN−(Al,Ga)N core−shell NW with a core diameter of 60 nm and a shell thickness of 46 nm. (b) Simulated strain profile of ε_{zz} for two different core−shell sizes.

core diameter of 60 nm and a shell thickness of 46 nm near the Γ-point. Due to the intrinsic doping of GaN, the Fermi level E_F is located close to the conduction band. Based on the band offsets between the materials involved a downward band bending of both valence and conduction band occurs within the core toward the GaN/(Al,Ga)N interface, which leads to an accumulation of electrons in that area. In addition, the different valence bands, namely, A, B, and C valence bands, vary energetically from each other. For unstrained GaN, the A valence band is known to be the energetically highest band and therefore responsible for radiative recombination.[19] However,

DOI: 10.1021/acs.nanolett.6b03354
Nano Lett. 2016, 16, 7098−7106

in the present case the mismatch-induced strain affects the energetic positions of the bands, which leads to an effective lowering of the A band below the C valence band, accompanied by an effective increase of the direct band gap. This trend has also been observed by Jacopin et al., who have simulated the band structure of GaN−AlN core−shell heterostructures via a 6 × 6 $\vec{k} \cdot \vec{p}$ method.[28] Accordingly, a value for the direct band gap of strained GaN can be obtained from the difference between conduction band and C valence band at the core center. Since both bands are almost parallel, this can be regarded as a good approximation for further studies.

In the following, the corresponding strain within the heterostructure is discussed. Since strain along the nonpolar *a*-direction (ε_{xx}, ε_{yy}) is mainly present at the capped top facet of the core−shell NW, the contribution to the overall strain system along the GaN core can be neglected in this study.[12,13,28] Thus, only the strain originating from the lattice mismatch along the polar *c*-direction, ε_{zz}, is further considered. In Figure 6b, the simulated strain across the heterointerfaces is displayed for two different core−shell sizes. The blue curve corresponds to the simulation in Figure 6a. A negative strain ε_{zz} occurs within the GaN core, whereas a positive value is obtained in the shell. This is equivalent to compressive and tensile strain in the core and the shell, respectively, which are responsible for changes in the band structure and consequently the band gap energy. For equivalent shell thicknesses but a larger core diameter (red curve) the absolute value of the strain within the core decreases accompanied by an increase in the shell. Consequently, this decreases the strain shift of the electronic bands of the GaN core, resulting in a less pronounced blueshift. The reason for this variation of the strain profile is a different distribution of elastic energy in the core and the shell, where the larger crystal applies a large force on the smaller one and vice versa. Next, the experimental results from our PL and Raman measurements are compared to the numerical simulations. To exclude any uncertainties during growth, i.e., variations in core and shell size, the dimensions of each core−shell array have been measured accurately and applied as input parameters for simulations. To directly determine these values from the investigated samples, the remaining pillars from the AFM releasing step have been analyzed by top view SEM images, where a distinct contrast can be identified between the core and the shell material (Figure 1c,d insets). As a result, the core diameters match well to the already employed values for all previous diagrams thanks to the high reproducibility of the GaN NW SAG process. However, the nominal shell thicknesses measured from top view SEM images of NW caps (Table 1) overestimate the actual shell thicknesses along the NW sidewalls by about 10−15 nm. Moreover, a decrease of the shell thickness from 50 to about 30 nm from the smallest to the largest core diameter has been observed. A possible explanation of this core-size-dependent shell growth could be the N-rich growth conditions, equivalent to a limiting supply of group III atoms during nucleation. Depending on the diffusion length of Al and Ga atoms, this can cause an effective decrease of the shell thickness for larger cores. However, this is in contrast to the constant cap thickness at the NW top facet, where the same effect would be expected. Another reason could be strain itself, leading to a size-dependent growth rate attenuation. As mentioned above, tensile strain within the shell increases with larger core diameters. Thus, the *c* lattice parameter of the (Al,Ga)N shell is stretched along the NW, which leads to an imperfect distance of lattice sites and thus to a possible perturbation of adatomic incorporation. As a consequence, the lateral growth rate of the shell decreases for larger core diameters, whereas the relaxed cap is free of any strain coming from the core.

In Figure 7a, experimental PL measurements of two different shell alloys (samples D and F, Table 1) are compared to

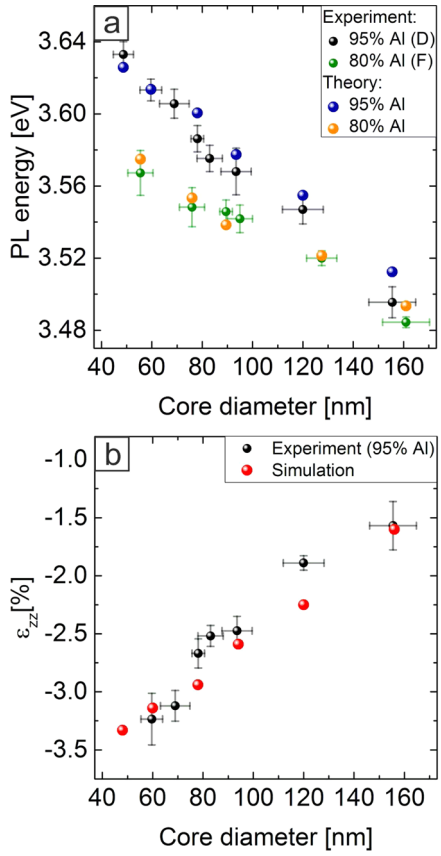

Figure 7. (a) Experimental PL peak energies for two different shell alloy compositions and (b) calculated core strain in growth direction from Raman measurements of sample D with corresponding theoretical values as a function of core diameter. The experimentally observed variation of the shell thickness is taken into account for these simulations.

simulated band gaps of the respective structures. For both alloy compositions of the shell the simulated values of the band gap follow well the experimental data sets. Small discrepancies with a tendency to higher energies in the case of the simulations can be either uncertainties in the theoretical input parameters or the experimentally obtained alloy compositions, or partial relaxation due to defects within the heterostructure. However, since most of the values agree within the error bars, it can be assumed that strain relaxation within the shell is not a main issue for these structures.

As a complementary verification, the simulated strain has been compared with Raman measurements of sample D. As indicated above, the shift Δk of the E_2^{high} mode of GaN is a reliable measure for strain.[20] In a good approximation, it can be assumed that $\Delta k = -2a \cdot \varepsilon_{xx} - b \cdot \varepsilon_{zz}$ where *a* and *b* are the so-called phonon deformation potential constants.[29] In the present case this can be simplified to $\Delta k \approx -b \cdot \varepsilon_{zz}$ where lateral strain contributions ε_{xx} can be neglected. Consequently, an experimental value from Raman measurements for ε_{zz} can be directly calculated for a given value of the parameter *b*. There

DOI: 10.1021/acs.nanolett.6b03354
Nano Lett. 2016, 16, 7098−7106

are many reports in the literature dealing with this parameter, involving a large variation from 727 to 965 cm^{-1}.[29−32] In the present study, a value of b = 797 cm^{-1} from Demangeot et al. matches well to the simulations of ε_{zz}, as shown in Figure 7b.[30] In particular, the simulated strain follows the experimentally obtained values with a similar slope, with any deviations again being mainly within the error bars. This is in agreement with the previous investigation of the band gap (Figure 7a), which underlines the assumption that strain relaxation plays a minor role for the investigated structures.

As a result, the simulated values for the band gap and the strain follow the experimental data from PL and Raman with a remarkably good agreement. Hestroffer et al. were able to show relaxation free core−shell growth up to 12 nm shell thickness but have claimed that the theoretical thickness limit must be several tens of nanometers.[12] Our results confirm this assumption, where the largest shell thickness of 50 nm still produces relaxation-free core−shell structures. As a consequence, the investigated SAG GaN−(Al,Ga)N core−shell NWs can serve as a model system for strain in three-dimensional heterostructures on the nanoscale.

Conclusion. We use the successful heteroepitaxial selective area growth of GaN−(Al,Ga)N core−shell nanowire heterostructures on Si(111) with a full control of nanowire period and location, core diameter, shell thickness, and alloy composition of the shell for a quantitative investigation of strain in these core−shell nanowires. Photoluminescence measurements on as-grown nanowires with different core−shell specifications on the same sample show a tuning of the free-exciton-emission of GaN up to 3.64 eV at room temperature for decreasing core diameter. Raman measurements reveal corresponding energy shifts of the E_2^{high} optical phonon mode, which confirm that compressive strain within the GaN core is exclusively responsible for the change in the band gap energy. In addition, the nanowire array period plays an important role for the morphology of the shell layer. For dense arrays the nanowires adopt a cone shape due to shadowing effects during growth. This affects the overall strain system within the core−shell nanowire leading to a less pronounced strain-induced blueshift. Thus, easily controlled nanowire parameters in selective area epitaxy such as core diameter and array period can be used to locally tune the band gap emission between 3.40 and 3.64 eV on one sample in only one growth cycle.

On the nanoscale, cathodoluminescence measurements demonstrate comparably small fluctuations of the near-band-edge emission by 20 meV along the nanowire core and prove the high homogeneity of the core−shell strain system.

Finally, the experimental findings are compared to numerical strain and band structure simulations for a large variety of core−shell configurations. Both, experiment and simulation agree with each other to a remarkably high degree. This is only possible by an absence of considerable strain relaxation via structural defects and confirms the high uniformity of the (Al,Ga)N shell growth and, in particular, the advantages of heteroepitaxial selective area growth compared to other nanowire growth techniques.

■ ASSOCIATED CONTENT

Supporting Information

The Supporting Information is available free of charge on the ACS Publications website at DOI: 10.1021/acs.nanolett.6b03354.

PL and CL spectra of the (Al,Ga)N shell. Simulations of the penetration depth of electrons in CL to determine the spatial resolution. High-resolution STEM study of the GaN/(Al,Ga)N interface (PDF)

■ AUTHOR INFORMATION

Corresponding Authors

*E-mail: martin.hetzl@wsi.tum.de.

*E-mail: stutz@wsi.tum.de.

Notes

The authors declare no competing financial interest.

■ ACKNOWLEDGMENTS

Financial support from the Deutsche Forschungsgemeinschaft (DFG) via the Forschergruppe 1493, TUM.solar in the frame of the Bavarian Collaborative Research Project "Solar technologies go Hybrid" (SolTec), the excellence cluster Nanosystems Initiative Munich (NIM), and the Fonds National Suisse de la Recherche Scientifique (FNS) through the National Centre of Competence in Research (NCCR) "QSIT - Quantum Science and Technology" is gratefully acknowledged. Further we want to thank the Centre Interdisciplinaire de Microscopie Électronique (CIME) for the access to the CL microscope.

■ REFERENCES

(1) Calleja, E.; Sánchez-García, M. A.; Sánchez, F. J.; Calle, F.; Naranjo, F. B.; Muñoz, E.; Jahn, U.; Ploog, K. *Phys. Rev. B: Condens. Matter Mater. Phys.* **2000**, *62*, 16826−16834.

(2) Schuster, F.; Furtmayr, F.; Zamani, R.; Magén, C.; Morante, J. R.; Arbiol, J.; Garrido, J. A.; Stutzmann, M. *Nano Lett.* **2012**, *12*, 2199.

(3) Wölz, M.; Hauswald, C.; Flissikowski, T.; Gotschke, T.; Fernández-Garrido, S.; Brandt, O.; Grahn, H. T.; Geelhaar, L.; Riechert, H. *Nano Lett.* **2015**, *15*, 3743−3747.

(4) Kumaresan, V.; Largeau, L.; Oehler, F.; Zhang, H.; Mauguin, O.; Glas, F.; Gogneau, N.; Tchernycheva, M.; Harmand, J.-C. *Nanotechnology* **2016**, *27*, 135602.

(5) Hersee, S.; Fairchild, M.; Rishinaramangalam, A.; Ferdous, M.; Zhang, L.; Varangis, P.; Swartzentruber, B.; Talin, A. *Electron. Lett.* **2009**, *45*, 75−76.

(6) Duan, X.; Huang, Y.; Agarwal, R.; Lieber, C. M. *Nature* **2003**, *421*, 241−245.

(7) Consonni, V.; Feuillet, G. *Wide Band Gap Semiconductor Nanowires*, 1st ed.; John Wiley & Sons, Inc., 2014; Chapter 3.

(8) Calarco, R.; Stoica, T.; Brandt, O.; Geelhaar, L. *J. Mater. Res.* **2011**, *26*, 2157−2168.

(9) Schuster, F.; Winnerl, A.; Weiszer, S.; Hetzl, M.; Garrido, J. A.; Stutzmann, M. *J. Appl. Phys.* **2015**, *117*, 044307.

(10) Schuster, F.; Hetzl, M.; Weiszer, S.; Wolfer, M.; Kato, H.; Nebel, C. E.; Garrido, J. A.; Stutzmann, M. *J. Appl. Phys.* **2015**, *118*, 154303.

(11) Armstrong, A.; Li, Q.; Lin, Y.; Talin, A. A.; Wang, G. T. *Appl. Phys. Lett.* **2010**, *96*, 163106.

(12) Hestroffer, K.; Mata, R.; Camacho, D.; Leclere, C.; Tourbot, G.; Niquet, Y. M.; Cros, A.; Bougerol, C.; Renevier, H.; Daudin, B. *Nanotechnology* **2010**, *21*, 415702.

(13) Rigutti, L.; Jacopin, G.; Largeau, L.; Galopin, E.; De Luna Bugallo, A.; Julien, F. H.; Harmand, J.-C.; Glas, F.; Tchernycheva, M. *Phys. Rev. B: Condens. Matter Mater. Phys.* **2011**, *83*, 155320.

(14) Hetzl, M.; Schuster, F.; Winnerl, A.; Weiszer, S.; Stutzmann, M. *Mater. Sci. Semicond. Process.* **2016**, *48*, 65−78.

(15) Schuster, F.; Hetzl, M.; Weiszer, S.; Garrido, J. A.; de la Mata, M.; Magen, C.; Arbiol, J.; Stutzmann, M. *Nano Lett.* **2015**, *15*, 1773.

(16) Sekiguchi, H.; Kishino, K.; Kikuchi, A. *Appl. Phys. Express* **2008**, *1*, 124002.

DOI: 10.1021/acs.nanolett.6b03354
Nano Lett. 2016, 16, 7098−7106

(17) Furtmayr, F.; Vielemeyer, M.; Stutzmann, M.; Arbiol, J.; Estradé, S.; Peirò, F.; Morante, J. R.; Eickhoff, M. *J. Appl. Phys.* **2008**, *104*, 034309.
(18) Iliopoulos, E.; Ludwig, K. F.; Moustakas, T. D.; Chu, S. N. G. *Appl. Phys. Lett.* **2001**, *78*, 463−465.
(19) Chen, G. D.; Smith, M.; Lin, J. Y.; Jiang, H. X.; Wei, S.; Asif Khan, M.; Sun, C. J. *Appl. Phys. Lett.* **1996**, *68*, 2784−2786.
(20) Kisielowski, C.; Krüger, J.; Ruvimov, S.; Suski, T.; Ager, J. W.; Jones, E.; Liliental-Weber, Z.; Rubin, M.; Weber, E. R.; Bremser, M. D.; Davis, R. F. *Phys. Rev. B: Condens. Matter Mater. Phys.* **1996**, *54*, 17745−17753.
(21) Vurgaftman, I.; Meyer, J. R. *J. Appl. Phys.* **2003**, *94*, 3675−3696.
(22) Consonni, V.; Hanke, M.; Knelangen, M.; Geelhaar, L.; Trampert, A.; Riechert, H. *Phys. Rev. B: Condens. Matter Mater. Phys.* **2011**, *83*, 035310.
(23) Zhang, X.; Rich, D. H.; Kobayashi, J. T.; Kobayashi, N. P.; Dapkus, P. D. *Appl. Phys. Lett.* **1998**, *73*, 1430−1432.
(24) Conesa-Boj, S.; Hauge, H. I. T.; Verheijen, M. A.; Assali, S.; Li, A.; Bakkers, E. P. A. M.; Fontcuberta i Morral, A. *Nano Lett.* **2015**, *15*, 2974−2979.
(25) Birner, S.; Zibold, T.; Andlauer, T.; Kubis, T.; Sabathil, M.; Trellakis, A.; Vogl, P. *IEEE Trans. Electron Devices* **2007**, *54*, 2137−2142.
(26) Vurgaftman, I.; Meyer, J. R.; Ram-Mohan, L. R. *J. Appl. Phys.* **2001**, *89*, 5815−5875.
(27) Ambacher, O.; Majewski, J.; Miskys, C.; Link, A.; Hermann, M.; Eickhoff, M.; Stutzmann, M.; Bernardini, F.; Fiorentini, V.; Tilak, V.; Schaff, B.; Eastman, L. F. *J. Phys.: Condens. Matter* **2002**, *14*, 3399.
(28) Jacopin, G.; Rigutti, L.; Bellei, S.; Lavenus, P.; Julien, F. H.; Davydov, A. V.; Tsvetkov, D.; Bertness, K. A.; Sanford, N. A.; Schlager, J. B.; Tchernycheva, M. *Nanotechnology* **2012**, *23*, 325701.
(29) Davydov, V. Y.; Averkiev, N. S.; Goncharuk, I. N.; Nelson, D. K.; Nikitina, I. P.; Polkovnikov, A. S.; Smirnov, A. N.; Jacobson, M. A.; Semchinova, O. K. *J. Appl. Phys.* **1997**, *82*, 5097−5102.
(30) Demangeot, F.; Frandon, J.; Renucci, M.; Briot, O.; Gil, B.; Aulombard, R. *Solid State Commun.* **1996**, *100*, 207−210.
(31) Wagner, J.-M.; Bechstedt, F. *Appl. Phys. Lett.* **2000**, *77*, 346−348.
(32) Gleize, J.; Renucci, M. A.; Frandon, J.; Bellet-Amalric, E.; Daudin, B. *J. Appl. Phys.* **2003**, *93*, 2065−2068.

DOI: 10.1021/acs.nanolett.6b03354
Nano Lett. 2016, 16, 7098−7106